Article

aeroacoustics

International Journal of Aeroacoustics
2017, Vol. 16(4–5) 431–456

DOI: 10.1177/1475472X17718883
journals.sagepub.com/home/jae
SAGE

A unified formalism for acoustic imaging based on microphone array measurements

Q Leclère,[1] A Pereira,[2] C Bailly,[2] J Antoni[1] and C Picard[3]

Abstract

The problem of localizing and quantifying acoustic sources from a set of acoustic measurements has been addressed, in the last decades, by a huge number of scientists, from different communities (signal processing, mechanics, physics) and in various application fields (underwater, aero, or vibro acoustics). This led to the production of a substantial amount of literature on the subject, together with the development of many methods, specifically adapted and optimized for each configuration and application field, the variety and sophistication of proposed algorithms being sustained by the constant increase in computational and measurement capabilities. The counterpart of this prolific research is that it is quite tricky to get a clear global scheme of the state of the art. The aim of the present work is to make an attempt in this direction, by proposing a unified formalism for different well known imaging techniques, from identification methods (acoustic holography, equivalent sources, Bayesian focusing, Generalized inverse beamforming...) to beamforming deconvolution approaches (DAMAS, CLEAN). The hypothesis, advantages and pitfalls of each approach will be established from a theoretical point of view, with a particular effort in trying to separate differences in the problem definition (a priori information, main assumptions) and in the algorithms used to find the solution. Numerical simulations will be proposed for different source configurations (coherent/incoherent/extended/sparse distributions), and an experimental illustration on a supersonic jet will be finally discussed.

Keywords

Microphone arrays, acoustic imaging, beamforming, deconvolution

Date received: 14 January 2017; revised: 26 March 2017; accepted: 22 April 2017

[1]University of Lyon, INSA-Lyon, Laboratoire Vibrations Acoustique, Villeurbanne, France
[2]University of Lyon, Ecole Centrale de Lyon, LMFA UMR CNRS 5509, Ecully, France
[3]MicrodB, Écully, France

Corresponding author:
Q Leclère, INSA-Lyon, University of Lyon, Laboratoire Vibrations Acoustique, Villeurbanne, F-69621, France.
Email: quentin.leclere@insa-lyon.fr

Introduction

A common problem in acoustics is the need for characterizing sources of sound or noise. Examples of such characterization are the estimation of direction-of-arrival of sound waves, the precise location of a source, its directivity, the spatial reconstruction of the source radiation pattern, the quantification/ranking of the acoustical power from different sources, among others. It often happens that measurements on the source itself are not practical and a well-established practice is to sense propagating acoustical waves coming from the source by means of an array of sensors. The idea behind this is to use the information gathered by the array together with a model of the propagation path to infer on source parameters. The inconvenient is that measurements are discrete in space due to practical reasons (mainly cost and hardware) and measuring all over a surface surrounding the source is barely feasible. Shortly stated, the aim of the methods discussed in this paper is thus to recover (estimate) parameters of noise sources from partial measurements of their radiated sound field.

Several researchers have been working on this subject for many decades[1](published research in the acoustics community has been seen since the pioneering work of Billingsley and Kinns[2] in the 70s). Applications of array processing on real-life problems cover a variety of domains (just in acoustics!) such as: underwater acoustics, speech, aero-acoustics, structural acoustics or ultrasound. Needless to say that array signal processing in general also finds its use in many fields of science, ranging from geophysics (seismology), radio astronomy up to bio-medical applications. A direct consequence is that original methods (aimed to particular applications) are constantly being developed, following the advances in computational and experimental resources. Due to the large amount of available techniques for processing array data aimed to source characterization, it is probably too ambitious to give a detailed description of the state of the art. Rather than providing an exhaustive list of existing methods, one goal of this work is to class different approaches by setting a unified formalism. Starting from the same formulation of the problem (precisely estimation of source parameters), the aim is to explicit the different branches (extensions) followed by each technique to achieve the solution. In other words, to specify which particular case of the original problem each method is trying to solve. One motivation is to allow the end-user to better choose which combination of algorithm/formulation fits best to a particular objective.

In this paper, the attention is mainly focused on techniques which provide an "image" (or map) of the acoustical source field of interest, thus the label *acoustic imaging techniques*. The majority of published methods in this domain may be divided into two main groups: beamforming-type and inverse problem-type methods. Distinction which is based on how the multiple degrees of freedom (i.e. source parameters to estimate) are treated. Notice that the term *identification* is also used in the literature to group methods based on an inverse problem formulation. This reasoning is followed on the next sections of the paper, in which references are given to well-known methods along with a discussion on their main assumptions, advantages and limitations.

The remainder of the paper is organized as follows. In next section, the problem of interest is formulated as the relation between a set of discrete "field" measurements (typically acoustical pressure or particle velocity) and source parameters (typically amplitude and location), by assuming that the propagation path is *known*. Then, the different "paths" taken to solve the problem of interest as well as computational aspects of the methods are given. Numerical simulations are then used in the following section with the aim of testing available methods on different source scenarios (e.g. mutually coherent/incoherent sources, extended/narrow source spatial distribution). In the last section, an experimental application is proposed, with a discussion on the diversity of results obtained through the different methods.

Formulation of the problem

In the frequency domain, the acoustic localisation problem is based on a linear relationship between a set of m acoustic pressure measurement points $\mathbf{p}$ and a set of n source strengths to be determined $\mathbf{q}$

$$\mathbf{p} = \mathbf{G}\mathbf{q} \tag{1}$$

where $\mathbf{G}$ $(m \times n)$ represents the acoustic transfer matrix, that depends on the frequency, the source definition and propagation medium. The sources can be defined as plane waves, (plane wave beamforming,[2] nearfield acoustic holography (NAH),[3] statistically optimized NAH (SONAH)[4]), spherical harmonics (HELS),[5] vibration velocity of numerical models (inverse boundary element method IBEM[6]), or a cloud of monopoles (spherical wave beamforming,[7,8] equivalent source methods[9–11]). The propagation medium is described by its acoustic celerity, with Sommerfeld boundary conditions (free field). It means that no reflection or diffraction is considered, except for the reflection and diffraction of the source itself, for the particular case of the IBEM. Note that an infinite reflective plane can, however, be taken into account quite easily, using an image source model (see Leclere et al.[12] for instance).

The computation of $\mathbf{p}$ from a known source $\mathbf{q}$, through equation (1), is called the direct problem: the effects (acoustic field) are estimated from the causes (sources). The estimation of $\mathbf{q}$ from $\mathbf{p}$ is thus an inverse problem, and suffers from several difficulties related to its ill-posed nature (non-uniqueness of the solution, high sensitivity to measurement noise). Generally speaking, a solution is expressed also with a linear system

$$\tilde{\mathbf{q}} = \mathbf{W}\mathbf{p} \tag{2}$$

where elements of $\tilde{\mathbf{q}}$ are the estimated source strengths and where the inverse operator $\mathbf{W}$ $(n \times m)$ depends not only on the chosen approach (assumptions, quantities to minimize, *a priori* information) but also in most cases on the measured quantities $\mathbf{p}$. Note that columns of matrix $\mathbf{W}'$ are called steering vectors in the beamforming literature (with $\mathbf{W}'$ the complex conjugate transpose of $\mathbf{W}$).

In equations (1) and (2), $\mathbf{p}$, $\mathbf{q}$ and $\tilde{\mathbf{q}}$ are complex-valued vectors, that represent the Fourier transformed data of a single time snapshot. Alternatively, they can be assessed from statistically stationary measurements using a phase reference, in the case of fully coherent measurements. However, a more general way to tackle stationary measurements is to directly formulate the direct and inverse problems in terms of auto and cross power spectral densities (PSD) averaged over several snapshots (time blocks)

$$\mathbf{S_p} = \mathbf{G}\mathbf{S_q}\mathbf{G}', \qquad \tilde{\mathbf{S}}_\mathbf{q} = \mathbf{W}\mathbf{S_p}\mathbf{W}' \tag{3}$$

where superscript $'$ denotes the complex conjugate transpose, and $\mathbf{S_p}$ and $\mathbf{S_q}$ (resp. $\tilde{\mathbf{S}}_\mathbf{q}$) are matrices of auto (diagonal terms) and cross (off-diagonal terms) spectra of measurements and (resp. estimated) sources.

The aim of the next section is to present briefly the various ways of estimating matrix $\mathbf{W}$.

Building the inverse operator

Data-independent beamforming

The output of standard beamforming is based on a least squares (LS) resolution of n independent systems relating the pressure vector $\mathbf{p}$ to the n-th entry in $\mathbf{q}$ through the n-th column of $\mathbf{G}$. This is done by using either plane or spherical waves: the strength of each candidate source is estimated independently from the others, in the LS sense. This leads to

$$\mathbf{W} = \ulcorner \mathbf{R} \lrcorner \mathbf{G}' \ulcorner \mathbf{L} \lrcorner \tag{4}$$

where $\mathbf{G}'$ is the complex conjugate transpose of the direct problem matrix $\mathbf{G}$, and $\ulcorner \mathbf{L} \lrcorner$ and $\ulcorner \mathbf{R} \lrcorner$ are diagonal matrices of positive weights equal to $\mathbf{I}$ for the simplest formulation. $\ulcorner \mathbf{L} \lrcorner$ consists of weights attributed to microphones (typically a spatial window), and $\ulcorner \mathbf{R} \lrcorner$ are source scaling terms. The classical LS solution leads to the choice of source scaling terms equal to the inverse squared norm of columns of $\mathbf{G}$[8], but other scaling strategies can be applied, to compensate for the effects due to large differences between averaged source-microphone distances, for instance Pereira and Leclere.[13] It is important to note that beamforming only gives an estimation of source strength at each focusing point as if it was the only source in the search grid, and thus cannot be directly re-introduced in equation (1). A global scaling can be applied afterward, but it is generally adjusted depending on the data.[12]

Data-dependant beamforming

A well-known data-dependent beamforming formulation is called minimum variance distortionless response (MVDR, also known as Capon[14,15]). For each candidate point source i, the corresponding line in matrix $\mathbf{W}$, noted $\mathbf{W}_{i:}$ is chosen to minimize $\mathbf{W}_{i:}\mathbf{S}_\mathbf{p}\mathbf{W}'_{i:}$ while keeping $\mathbf{W}_{i:}\mathbf{G}_{:i} = 1$ ($\mathbf{G}_{:i}$, is the i-th column of matrix $\mathbf{G}$). It can be seen as a way of minimizing the contribution of all sources except source i. The optimum is given by[16]

$$\mathbf{W}_{i:} = \frac{\mathbf{G}'_{:i}\mathbf{S}_\mathbf{p}^{-1}}{\mathbf{G}'_{:i}\mathbf{S}_\mathbf{p}^{-1}\mathbf{G}_{:i}} \tag{5}$$

or, in a matrix form

$$\mathbf{W} = \mathrm{Dg}\left(\mathbf{G}'\mathbf{S}_\mathbf{p}^{-1}\mathbf{G}\right)^{-1}\mathbf{G}'\mathbf{S}_\mathbf{p}^{-1} \tag{6}$$

where $\mathrm{Dg}(\mathbf{A})$ is the diagonal matrix constituted of diagonal terms of $\mathbf{A}$.

A major assumption of this method is that all sources contributing to the measurements are uncorrelated, and it is very sensitive to violations of this hypothesis, or to a non-converged estimation of $\mathbf{S}_\mathbf{p}$.[17] The robustness of the approach is generally enforced by artificially loading the diagonal of $\mathbf{S}_\mathbf{p}$. It is interesting to note that in this case, equation (6) tends to a standard beamforming (equation (4)) as the diagonal loading factor increases. It is also possible to separate in $\mathbf{S}_\mathbf{p}$ the contribution of sources from the noise (using eigenvalue analysis, Bienvenu and Kopp[18]). Other modified versions can be obtained, to extend the method to potentially coherent sources.[19]

Inverse methods

Beamforming approaches aim at solving a scalar inverse problem: the strength of each source is identified independently from the others. The steering vectors (columns of $\mathbf{W}'$) are determined as a function of the source (position, angle of incidence), and then the beamformer is "scanned" over the source area covering the location of potential sources. Inverse methods, in contrast, consider the problem for all sources at once. The advantage of such approaches is that interferences between potential coherent sources are taken into account: the idea is to find the linear combination of sources (or the whole source covariance matrix) to obtain reconstructed pressures (through equation (1) or equation (3)) that are as close as possible to the measured ones. The choice on the nature of sources will define different methods in the literature, beginning with a basis of plane waves (including evanescent ones) for planar NAH or SONAH,[3,4] BEM-based radiation functions,[6] monopole distributions[9–11] or spherical harmonics.[5]

A common difficulty is that these methods can be very sensitive to measurement noise, and often require a regularization procedure. In addition, the inversion is generally underdetermined, because the number of microphones is limited due to practical aspects, and the number of source degrees of freedom (dofs) is thus often larger than the number of measurement points. These two issues are typical characteristics of ill-posed problems, in the sense of Hadamard.[20] A very common approach to handle this issue is known as Tikhonov regularization,[21] which is based on the minimization of both the standard LS error and the norm of the solution (source terms). The quantity to be minimized as a function of $\mathbf{q}$ is

$$||\mathbf{p} - \mathbf{G}\mathbf{q}||^2 + \eta^2||\mathbf{q}||^2 \tag{7}$$

where η^2 is the Tikhonov regularization parameter, which controls the trade-off between the minimization of the LS error and the solution's norm. When dealing with quadratic versions of the problem, i.e. involving cross spectral matrices (equation (3)), the quantity to be minimized can be formulated as follows

$$||\mathbf{P} - \mathbf{G}\mathbf{Q}||_F^2 + \eta^2||\mathbf{Q}||_F^2 \tag{8}$$

where $\mathbf{Q}$ is a $(n \times m)$ matrix to be determined (with $\mathbf{Q}\mathbf{Q}' = \mathbf{S_q}$) and $||\;||_F$ denotes the Frobenius norm. Matrix $\mathbf{P}$ is a $(m \times m)$ matrix such that

$$\mathbf{P}\mathbf{P}' = \mathbf{S_p} \tag{9}$$

The matrix $\mathbf{W}$ allowing to obtain the solution of this minimization problem is

$$\mathbf{W} = \mathbf{G}^{+\eta} = \mathbf{G}'\left(\mathbf{G}\mathbf{G}' + \eta^2\mathbf{I}\right)^{-1} \tag{10}$$

$\mathbf{G}^{+\eta}$ denoting the regularized pseudo-inverse of $\mathbf{G}$. The difficulty is to choose correctly the parameter η^2. Various automated methods exist for this purpose, such as the general cross validation,[22] the L-curve[23] or more recently a Bayesian criterion[11] which shows better robustness than the former two methods for the inverse acoustic problem.[24] It is also possible to add left and right weighting matrices, as it is the case for beamforming (matrices $\mathbf{L}$ and $\mathbf{R}$ in equation (4)), to adjust the importance given to either microphone or source dofs in the minimization problem (8). These matrices are, however, skipped here for the sake of simplicity.

Note that when η^2 tends to ∞, the pseudo-inverse tends towards the conjugate transpose (with a scaling factor η^{-2}), the over-regularized inverse method is thus similar to standard beamforming. In practice, the consequence is that the automated choice of η may select $\eta = 0$; this is the case when matrix $\mathbf{G}$ has a low condition number (generally at high frequencies). In this particular case, the pseudo inverse solves the following minimization problem (still assuming under-determined cases):

$$\text{Minimize } \operatorname{tr}\left(\mathbf{S_q}\right) \text{ subject to } \mathbf{G}\mathbf{S_q}\mathbf{G}' = \mathbf{S_p} \tag{11}$$

This problem is no more a trade-off, and its solution is simply the least norm one, among all solutions satisfying $\mathbf{G}\mathbf{S_q}\mathbf{G}' = \mathbf{S_p}$. It means that the method is not able to separate the noise from the signal in $\mathbf{S_p}$, it just gives as a result, among the infinity of potential exact solutions, the minimum norm one. Practically speaking, consequences are that the results can strongly under-estimate the real source strengths. A solution to this problem is to add more *a priori* information, such as sparsity constraints. This is the subject of the next section.

It is worth noting that several methods are based on this inverse formulation, but have been developed in relatively disjoint scientific communities. Some approaches come from the aeroacoustics beamforming community, for which this approach is an improvement of beamforming (soap,[25] generalized beamforming[26]), and some others come from the acoustic inverse problem community (sonah,[4] ESM,[9,10] Bayesian focusing[11,24]). This formulation can somehow be understood as a kind of convergence of NAH-related methods and beamforming.

Sparsity constraints

A fundamental limitation of inverse formulations of the acoustic problem is due to the fact that they are generally underdetermined, because of the practically limited number of microphones used to sample the acoustic field, that is often much lower than the number of source degrees of freedom. The regularization principle to choose, among the infinite number of solutions, the one of minimal norm, is in this situation somewhat arbitrary, and has a tendency to give underestimated source powers. It is shown in Pereira[27] and Pereira et al.[28] that identified sources have radiation patterns directed towards the array. That's why source powers are systematically underestimated, especially at high frequencies when the optimal regularization parameter is equal to 0 (yet the localization ability remains generally satisfying). Note that this effect is also mentioned in the plane-wave version of the method (sonah[4]).

The correct quantification of source powers thus requires the addition of *a priori* information about the source. This can be done by assuming that the source distribution may be represented by only a few non-zero components, in a given basis. In this case, the initial choice of elementary sources (monopoles, plane waves, spherical harmonics) used to build the direct operator $\mathbf{G}$ is fundamental, since it will determine in which basis the sparsity is assumed: this choice is equivalent to a priori assumptions on the nature of the source. The set of elementary sources is referred to as the *dictionary* in sparse modeling, and the image of each elementary source on the microphones (columns of $\mathbf{G}$) is called *atom* or *word.*

The simplest way to measure sparsity is the L_0 norm of the solution, corresponding here to the number of non-zero components on the diagonal of $\mathbf{S_q}$. However, the minimization of this quantity is not an easy task, from the mathematical point of view, because it corresponds to a non-convex problem: it requires a combinatory exploration of potential solutions that may be not unique. The L_0 minimization is thus often relaxed to the convex L_1 minimization problem, which is known to lead under some conditions to equivalent solutions.[29] It is in fact possible to adjust a level of sparsity, by using an L_p norm, with p varying between 1 (strong sparsity) and 2 (no sparsity). The identification problem with sparsity constraint is thus to find $\mathbf{q}$ minimizing the following quantity

$$||\mathbf{p} - \mathbf{G}\mathbf{q}||^2 + \eta^2 \sum_i |q_i|^p \tag{12}$$

where q_i is the *i-th* element of $\mathbf{q}$. When dealing with quadratic versions of the problem, assuming $\mathbf{S_{pp}} = \mathbf{P}\mathbf{P}'$, the quantity to be minimized can be formulated as follows

$$||\mathbf{P} - \mathbf{G}\mathbf{Q}||_F^2 + \eta^2 \sum_i \left(\sum_j |Q_{ij}|^2 \right)^{p/2} \tag{13}$$

where $\mathbf{Q}$ is a $(n \times m)$ matrix to be determined (with $\mathbf{Q}\mathbf{Q}' = \mathbf{S_q}$) and Q_{ij} the *i-th* element of the *j-th* column of $\mathbf{Q}$. Several approaches can be used to minimize equation (13), such as heuristics, iterative inverse methods and sparse optimization.

Heuristic solutions. As already stated, defining the sparsity constraint through the minimization of the L_0 norm of the solution leads to an optimization problem that is difficult to handle correctly. However, it is possible to apply very simple iterative methods to search for "not so bad" solutions, without any guarantee to find a global optimum. Heuristic approaches, such as (Orthogonal) Marching Pursuit,[30] offer such results with very simple algorithms. In acoustic imaging, several methods belong to this class (see for instance Wang et al.[31]).

An application of OMP to the quadratic form of the acoustic problem (equation (3)) can be formulated as follows. First, initial conditions are defined as

$$\Omega^{(0)} = \emptyset, \quad \mathbf{S_r}^{(0)} = \mathbf{S_p}$$

Then, for each $n \geq 1$, the following steps are iteratively operated:

- The support of the source Ω is enlarged by including the source dof maximizing the beamforming output of the residual matrix $\mathbf{S_r}$

$$\Omega^{(n)} = \Omega^{(n-1)} \cup \ \mathrm{argmax}_i \left(\mathbf{G}'_{:,\mathbf{i}} \mathbf{S_r}^{(n-1)} \mathbf{G}_{:,\mathbf{i}} \right)$$

- The inverse operator is calculated over the new support ($\mathbf{\Omega}^{(n)}$ standing for a Boolean matrix selecting source dofs included in the set $\Omega^{(n)}$ and $^+$ standing for the pseudo-inverse)

$$\mathbf{W}^{(n)} = \mathbf{\Omega}^{(n)} \left(\mathbf{G} \mathbf{\Omega}^{(n)} \right)^+$$

- The new source and residual matrices are finally updated

$$\mathbf{S}_{\mathbf{q}}^{(n)} = \mathbf{W}^{(n)}\mathbf{S}_{\mathbf{p}}\mathbf{W}^{(n)'}, \quad \mathbf{S}_{\mathbf{r}}^{(n)} = \mathbf{S}_{\mathbf{p}} - \mathbf{G}\mathbf{S}_{\mathbf{q}}^{(n)}\mathbf{G}'$$

The stopping criterion of this iterative process can either be a maximum number of iterations (maximum dimension of the support), the norm of the residual matrix, or the condition number of the pseudo-inversed matrix.

Iterative inverse methods. This family of methods is related to iterative reweighted least squares (IRLS[32,33]). The idea is starting from the classical problem (equation (8)) to inject a penalty term at iteration $n+1$ derived from source strengths at iteration n. In doing so, more and more weight is given to strong sources, to finally converge to a sparse result. Among the acoustic applications of this approach, we can cite the L1-generalized beamforming,[34,35]and Bayesian methods.[27,36] A comparison of these two approaches is realized in Oudompheng et al.[37] In the former, the possibility of using an overcomplete dictionary is illustrated by identifying jointly monopole and dipole distributions. In the latter, a direct link is done between the a priori law of the source distribution (a generalized Gaussian law) and the power p of the norm in equation (13). The inverse operator $\mathbf{W}$ can be expressed, at iteration $n+1$, as follows

$$\mathbf{W}_{(n+1)} = \mathbf{R}_{(n)}\left(\mathbf{G}\mathbf{R}_{(n)}\right)^{+\eta} = \mathbf{R}_{(n)}^2\mathbf{G}'\left(\mathbf{G}\mathbf{R}_{(n)}^2\mathbf{G}' + \eta^2\mathbf{I}\right)^{-1}$$

where $\mathbf{R}_{(n)}$ is a right diagonal weighting matrix, adjusting the importance given to the minimization of the contribution of each source, and that is computed using the solution at iteration n

$$[\mathbf{R}_{(n)}^2]_{i,i} = \left([\mathbf{S}_{\mathbf{q(n)}}]_{i,i}\right)^{1-p/2}$$

A study of the effect of p on the results of acoustic imaging problems is given in Leclere et al.[38]

Sparse optimization. Other methods search for global solutions through the minimization of the L1 norm of the solution (e.g. BPDN,[39] LASSO[40]). Several tools are available[41] to solve them and have also been implemented for acoustic imaging purposes.[38,42] However, a difficulty remains in finding solutions corresponding to the quadratic version of the problem (equation (3)). A possibility is to use the decomposition (9), and to process the sparse optimization independently for each component.[34,35] This is, however, not fully satisfying, because the L1 norm is not minimized globally, as it would be the case in considering jointly all diagonal terms of $\mathbf{S}_{\mathbf{q}}$ (note that this is different if there is more than one component, i.e. more than one statistically independent source).

Deconvolution methods

The acoustic imaging approaches presented in the previous sections aim at estimating the source strengths. This estimation is noted $\tilde{\mathbf{q}}$ considering equation (2) or $\tilde{\mathbf{S}}_{\mathbf{q}}$ considering equation (3). In this section, one considers the possibility to recover true values of $\mathbf{q}$

or $\mathbf{S_q}$, conditioned by additional assumptions. The use of equation (1) in equation (2) directly gives

$$\tilde{\mathbf{q}} = \mathbf{WGq}, \quad \tilde{\mathbf{S}}_\mathbf{q} = \mathbf{WGS_qG'W'} \tag{14}$$

This illustrates the fact that generally inverse methods are not exact, considering that **WG** is not equal to identity. In fact, columns of matrix **WG** are representing the output of the method to single unit sources. The columns of the matrix constituted of terms of **WG** in squared absolute values are called point spread functions, representing the power output of the method to unitary point sources

$$[\mathbf{A}]_{i,j} = \left|[\mathbf{WG}]_{i,j}\right|^2 \tag{15}$$

Assuming uncorrelated sources, equation (14) boils down to

$$\tilde{\bar{\mathbf{q}}}^2 = \mathbf{A}\bar{\mathbf{q}}^2 \tag{16}$$

where $\bar{\mathbf{q}}^2$ and $\tilde{\bar{\mathbf{q}}}^2$ represent the diagonals (autospectra) of $\mathbf{S_q}$ and $\tilde{\mathbf{S}}_\mathbf{q}$, respectively. The identification of $\bar{\mathbf{q}}^2$ from $\tilde{\bar{\mathbf{q}}}^2$ and **A** has been studied in Blacodon and Elias,[43] and is introduced as the DAMAS inverse problem in Brooks and Humphreys[44] (deconvolution approach for the mapping of acoustic sources). The approach is presented as a deconvolution problem, the aim being to remove from the source energy maps the blurring effects of the inverse operator.

It is noteworthy that the hypothesis of uncorrelated sources is generally assumed for using equation (14), as it is a sufficient one. However, this is not a strictly necessary one. Indeed, if coherent sources are far enough so that the spatial supports of their PSF are disjoint (or almost disjoint), equation (16) remains (almost) true. Problems are expected either in the low frequency range, where PSFs supports are wider due to low resolution, or when correlated sources are close to each other (typically radiating panels, or multipole sources).

Several ways exist to solve equation (14), for which an inversion under constraint is needed, because the result has to be positive (source autospectra). In the original work,[44] this problem is solved by using a Gauss–Seidel iterative algorithm, with a thresholding at each iteration to enforce the positivity of the result. The iteration is stopped after a given number of iterations, which has a significant effect on the result. Another way of solving equation (16) is the non-negative least squares.[45] Several approaches are compared in Ehrenfried and Koop.[46] Note that the inversion under the positivity constraint is relatively well-posed: regularization is not required and in addition, the results have a sparse aspect (only few components of $\tilde{\bar{\mathbf{q}}}^2$ are found non zero).

Sparse optimization and heuristic methods have also been implemented to solve this problem, related to matching pursuit (CLEAN,[47,48]OMP[49]), basis pursuit (SC-DAMAS[50]) or Bayesian formalism.[51] It is interesting to note that assuming the sparsity through a L_1 minimization of $\tilde{\bar{\mathbf{q}}}^2$ is equivalent to the L_2 norm used in Tikhonov's regularization (equation (8)). Consequently, the sparsity of the results can somehow be attributed more to the non-negativity constraint than to the sparsity constraint. The link between non negativity constraints and sparse results is discussed in Bruckstein et al.[52] and Foucart and Koslicki.[53]

CLEAN-PSF and CLEAN-SC[47,48] have become quite popular in the field of aeroacoustics in the last decade due to their robustness and computational efficiency. The idea is to iteratively remove from the measured pressures (a part of) the contribution of the beamforming map maximum. This contribution is computed differently for the two algorithms: CLEAN-PSF uses the Green function between the maximum position and the array, while CLEAN-SC uses the coherence between the maximum and the measured pressures on the array. CLEAN-PSF is thus basically equivalent to a Matching Pursuit algorithm. CLEAN-SC uses more advanced tools related to conditioned spectral analysis[54] where conditioning is performed iteratively with respect to a linear combination of microphones that corresponds to the steering vector pointing to the maximum of the residual beamforming map.

Global classification of acoustic imaging methods

A global classification of acoustic imaging approaches is proposed in Figure 1 to try to sum up all methods raised in previous sections. The proposed classification is separated first in either beamforming-related methods (for which each source dof is handled independently) or inverse methods (all source dofs are considered at once). Approaches are then classified, based on the definition of the minimization problem, and some corresponding methods/algorithms are appended in red font. Note that deconvolution is seen as a post processing of standard beamforming, for which additional hypotheses are assumed, and for which all source dofs are processed at once. Deconvolution belongs thus to the class of inverse problems, with an additional non-negativity constraint. That is why some algorithms are shared by deconvolution and inverse methods (typically greedy algorithms CLEAN, OMP...).

Numerical illustrations

Configuration

The studied configuration is drawn in Figure 2. A linear acoustic array (32 microphones, 70 cm length, non-regular spacing), is placed at 70 cm from a parallel linear source. Different

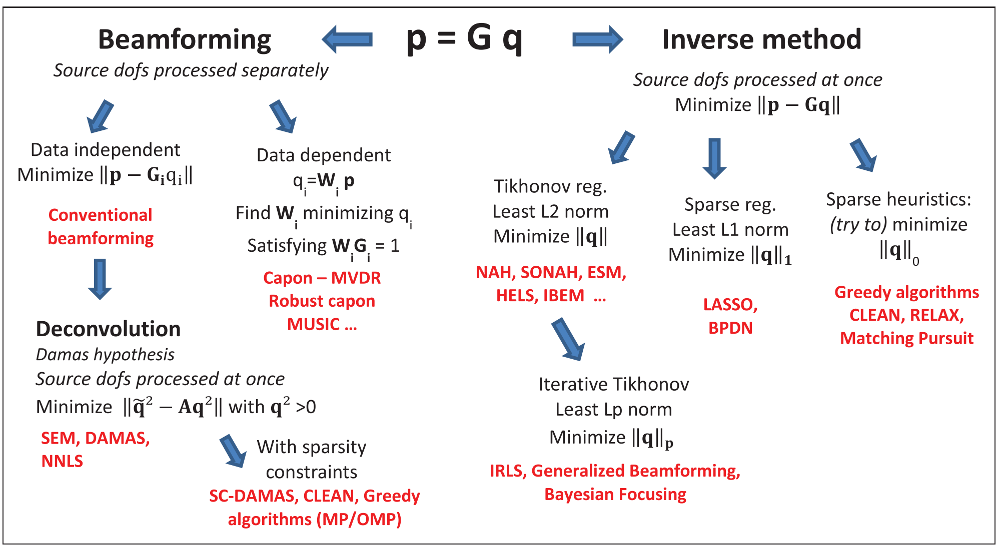

Figure 1. Global classification of acoustic imaging approaches.

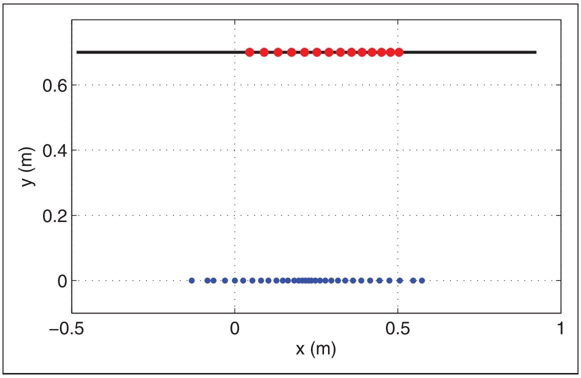

Figure 2. Simulated configuration. Blue dots: microphone positions. Black line: candidate sources. Red dots: actual source positions used in simulations 1 and 2 ('Uncorrelated monopoles' section and 'Correlated monopoles' section).

source configurations are tested in this work to illustrate the behavior of the different acoustic imaging methods presented in the theoretical part. The input of the simulation is a source spectral matrix $\mathbf{S_q}$, and the matrix of acoustic pressures is obtained thanks to equation (3). A cross spectral matrix of noise is added to the matrix of acoustic pressures. The noise is independent on each microphone, and its correlation matrix is randomly built at each frequency following asymptotic laws (cf. Leclere et al.[55] with 200 time snapshots). The signal to noise ratio is arbitrarily set to 10 dB. The interest of considering a 1D problem is that the results are easily represented as a function of the frequency on 2D maps, with the frequency on the first axis and the space on the second one. Simulations are carried out from 1 to 20 kHz with a step of 100 Hz. Results are presented systematically in the following section, for different methods introduced in this work:

- standard beamforming (cf. 'Data-independent beamforming' section, with terms of the source scaling matrix $\ulcorner \mathbf{L} \lrcorner$ equal to the inverse of the norm of the columns of $\mathbf{G}$),
- Orthogonal Matching Pursuit (cf. 'Heuristic solutions' section 3.4.1),
- Inverse method (Bayesian regularization, functional J_{MAP} in Pereira et al.,[24] 'Inverse methods' section),
- IRLS (Bayesian regularization 'Iterative inverse methods' section) with $p = 1$ and $p = 0$,
- deconvolution ('Deconvolution methods' section) with DAMAS (original algorithm,[44] 1000 iterations),
- deconvolution ('Deconvolution methods' section) with NNLS (solution of equation (16) using Matlab lsqnonneg function).
- CLEAN (CLEAN-PSF algorithm described in Sijtsma,[48] loop gain set to 0.1),
- CLEAN-SC (CLEAN based on source coherence Sijtsma,[48] loop gain set to 0.1.

The considered source configurations are:

- 14 uncorrelated monopoles (same amplitudes, positions given in Figure 2),
- 14 correlated monopoles (in phase, same amplitudes, positions given in Figure 2),

- uncorrelated uniform spatial distribution on interval [0; 0.5]m,
- correlated in phase uniform spatial distribution on interval [0; 0.5]m.

These configurations are inspired from an experimental application of acoustic imaging applied to jet noise,[56] that is addressed in the following section. Monopole positions correspond to the positions of cells, at the origin of the broadband shock noise. The uniform distribution could be representative of a turbulent mixing noise. Note that uniform distributions are practically constituted of monopoles with a high density (1 mm spacing, i.e. 500 sources between in the interval [0; 0.5]m).

Uncorrelated monopoles

Results for the configuration with uncorrelated monopoles are drawn in Figure 3. This configuration can be seen as favorable for all the methods: sources are really punctual and uncorrelated, which satisfies the hypothesis of conventional beamforming and deconvolution. In all cases, the results are generally better in the high frequency range, because of the resolution of imaging methods related to the acoustic wavelength. The sources that are closer to $x = 0$ are separated above 8 kHz, while sources around $x = 0.5$ are separated above 13 kHz. This observation, common to all results, is due to the fact that the distance between point sources decreases with x: from about 4.5 cm (wavelength at 7500 Hz) between the first two to 2.6 cm (wavelength at 13 kHz) between the last two, confirming the fact that two sources are separated when they are more than one acoustic wavelength away from each other. It is interesting to compare the low frequency behavior of all the methods, some of them giving a relatively distributed result (beamforming, inverse method, IRLS $p = 1$, DAMAS) while others give punctual results, but at erroneous places (OMP, IRLS $p = 0$, NNLS, CLEAN). The methods are also characterized by results with very different background noise and secondary lobes, for which the inverse method IRLS with $p = 0$ seems to give especially good results, as well as CLEAN-SC for which the energy recovered outside the actual source region is significantly lower than CLEAN-PSF.

Correlated monopoles

Results for the configuration with correlated monopoles are drawn in Figure 4. It is interesting to note, when looking at beamforming results, that the interferences complexify the source map (as compared to the previous case). It is thus expected that the deconvolution approaches, which assume that the source map is an energetic summation of PSFs, will meet with difficulties. However, similar remarks as for the previous case (uncorrelated sources) can be made: at low and mid frequency, the sources are not well separated for all methods. Some methods (Bayes $p = 2$, IRLS $p = 1$, Damas) return distributed sources, while others (Bayes $p = 0$, NNLS, CLEAN-PSF) lead to point sources at wrong locations. The frequency above which sources are separated is higher than in the previous case, illustrating the increased difficulty of the identification problem when sources are correlated. Once again, the method giving the most satisfying results in terms of dynamic range is IRLS $p = 0$. It is also noted that OMP, despite the simplicity of its implementation, gives quite good results at high frequencies as compared to deconvolution approaches. CLEAN-SC, as expected in this case, fails to identify several sources because of its implementation based on the source coherence. In this, configuration, sources are indeed fully correlated with one another, which means that all the signal is removed when applying spectral conditioning with respect to any point of the source map. That's why only one source is recovered by CLEAN-SC in such a situation.

Uncorrelated uniform distribution

The third source configuration consists of an incoherent line source between $x = [0, 0.5]$m, results are drawn in Figure 5. This source is constituted of a distribution of uncorrelated unitary monopoles, with a spatial resolution of 1 mm (500 sources). In this case, matrix $\mathbf{S_q}$ is a (500 × 500) identity matrix. The methods once again can be split into two families, a first one leading to a uniform distribution and a second one to clouds of point sources. Deconvolution approaches give good results, because of the satisfied hypothesis of independence between sources. Among deconvolution approaches, DAMAS only seems capable of recovering an almost uniformly distributed source. CLEAN also gives a continuous source in the high frequency range, thanks to a relatively low loop gain, equal to 0.1. It can be noted that deconvolution approaches, especially DAMAS and NNLS, are disturbed by strong secondary lobes outside the source area. IRLS ($p = 1$) offers an interesting compromise between the capability to recover a distributed source and a good dynamic range. NNLS as well as IRLS ($p = 0$) lead to clouds of monopoles well distributed in the support of the real source ($x = [0, 0.5]$m). However, once again, a characteristic distance is observed between punctual sources that depends upon the frequency. One must take special care not to interpret it as a property of the source, but as an effect of the method.

Correlated uniform distribution

The fourth source configuration consists of a line source between $x = [0, 0.5]$m, results are drawn in Figure 6. This source is constituted of a distribution of correlated unitary in-phase monopoles, with a spatial resolution of 1 mm (500 sources). This configuration can be seen as the 1D baffled piston case. A strong difference appears between inverse methods and deconvolution: inverse methods recover correctly the uniformity of the source strengths, while deconvolution approaches are characterized by a spatial envelope whose maximum around a value of $x \approx 0.2$ corresponds to the center of the array. Note that this envelope is already present on beamforming results, and not corrected by deconvolution. The inverse method ($p = 2$) and IRLS ($p = 1$) give spatially distributed results, with a better dynamic range for the latter. The DAMAS result is also somehow distributed, but not uniformly. Sparse approaches lead to a set of punctual sources instead of a distributed source, the number of which depending on the frequency: it is worth noting that this kind of result can lead to misinterpretations concerning the structure of the source distribution. CLEAN-SC returns, as expected, a unique source in this particular case of a fully correlated source distribution.

Acoustic power estimation

It is not straigthforward to compare results of acoustic imaging methods in terms of integrated source strength. It can be realized in terms of the acoustic power integrated by regions that can be obtained by calculating the acoustic power associated to each point of the source grid (monopole sources are considered here). This quantity depends on the source strength

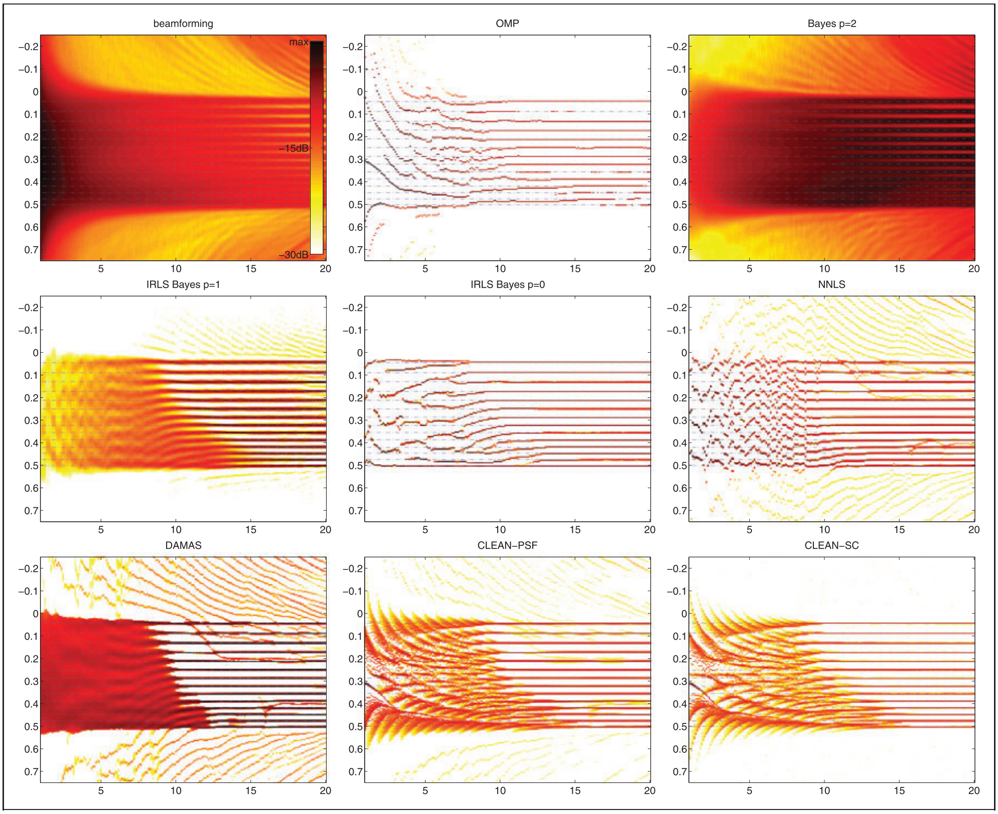

Figure 3. Configuration 1: Uncorrelated monopoles. Color dynamic 30 dB. Horizontal axis: Frequency in kHz, vertical axis: source position in meters.

of the *i-th* grid point q_i and on the pressure generated at the *i-th* source position by all other sources $\hat{p}_i$:

$$\begin{aligned} w_i &= \frac{1}{2\rho c}\left(\frac{|q_i|^2}{4\pi} - \frac{1}{k}\mathcal{I}(\hat{p}_i\overline{q_i})\right) \\ &= \frac{1}{2\rho c}\left(\frac{[\mathbf{S_q}]_{i,i}}{4\pi} - \frac{1}{k}\mathcal{I}\left(\sum_{j\neq i} g_{ij}[\mathbf{S_q}]_{j,i}\right)\right) \end{aligned} \tag{17}$$

where ρ, c, k stand, respectively, for the density, acoustic celerity and wavenumber of the medium at the considered frequency, and where $g_{ij} = \exp(-\imath k r_{ij}/(4\pi r_{ij}))$ is the Green's function of the point source between points i and j of the source grid separated by the distance r_{ij}.

This formulation is used here to obtain the acoustic power distributions from the results of inverse methods (OMP, Bayes, and IRLS Bayes), for which full source matrices $\mathbf{S_q}$ are estimated, and also to compute the actual acoustic power of the simulated source configuration. For deconvolution methods (DAMAS, NNLS, CLEAN-SC and CLEAN PSF), the hypothesis of source incoherence is admitted. The second term of equation (17) can thus be

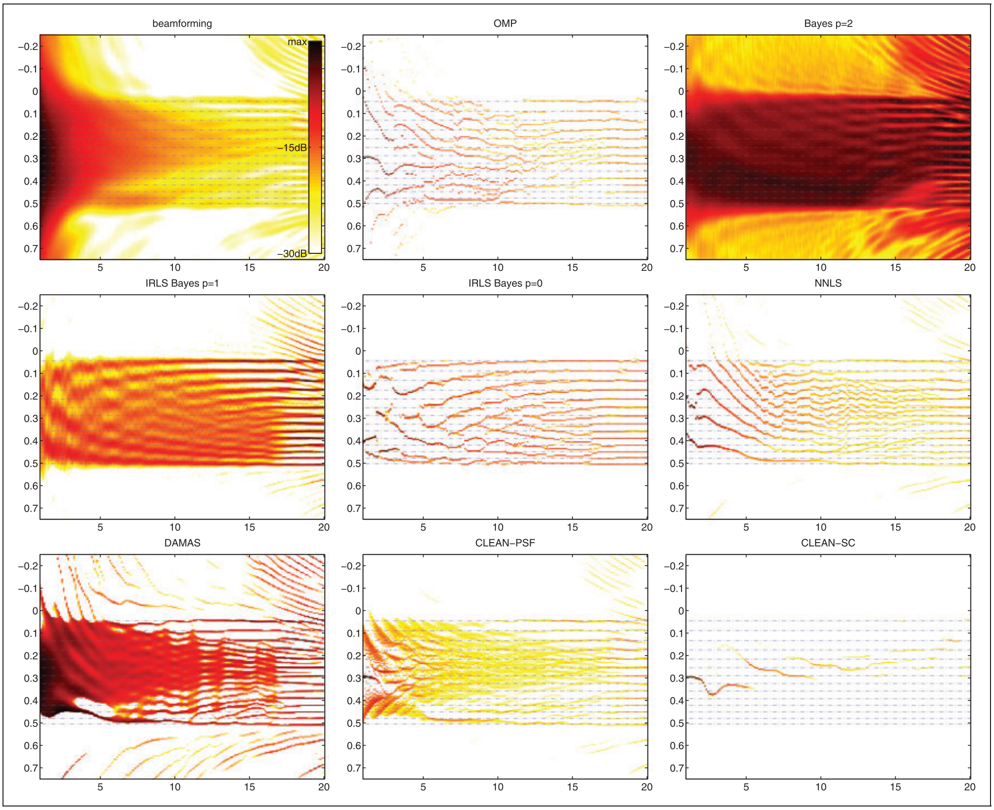

Figure 4. Configuration 2: Correlated monopoles. Color dynamic 30 dB. Horizontal axis: Frequency in kHz, vertical axis: source position in meters.

considered as equal to 0, the acoustic power associated to each point of the source grid being equal to $[\mathbf{S_q}]_{i,i}/(8\pi\rho c)$.

The acoustic power map obtained for each method is integrated between $0 < x < 0.6$ and compared to the true acoustic power. Ratio between the estimated and true values for each method is drawn in Figure 7 in dB, for all considered source configurations.

When dealing with uncorrelated source distributions (configurations 1 and 3), the deconvolution methods (NNLS, DAMAS, CLEAN), relying on the hypothesis of uncorreralted sources, are correctly assessing the input power. Inverse methods without or with a smooth sparsity constraint (Bayes $p = 2; 1$) are systematically underestimating the input power (approximately 5 dB or 3 dB for $p = 2$ and 1, respectively), as expected (see discussion at the end of 'Inverse methods' section). Inverse methods with a strong sparsity constraint (OMP, Bayes $p = 0$) do not suffer from this underestimation, but the robustness of the estimation is less good than deconvolution methods. However, the estimation error of the Bayesian approach with $p = 0$ remains lower than 1 dB on a very wide frequency range.

Concerning configurations with correlated sources (configurations 2 and 4), deconvolution results (NNLS, DAMAS, CLEAN-PSF) are overestimating the input power, only in the low frequency range (<8 kHz) for configuration 2 (correlated monopoles) and on the whole

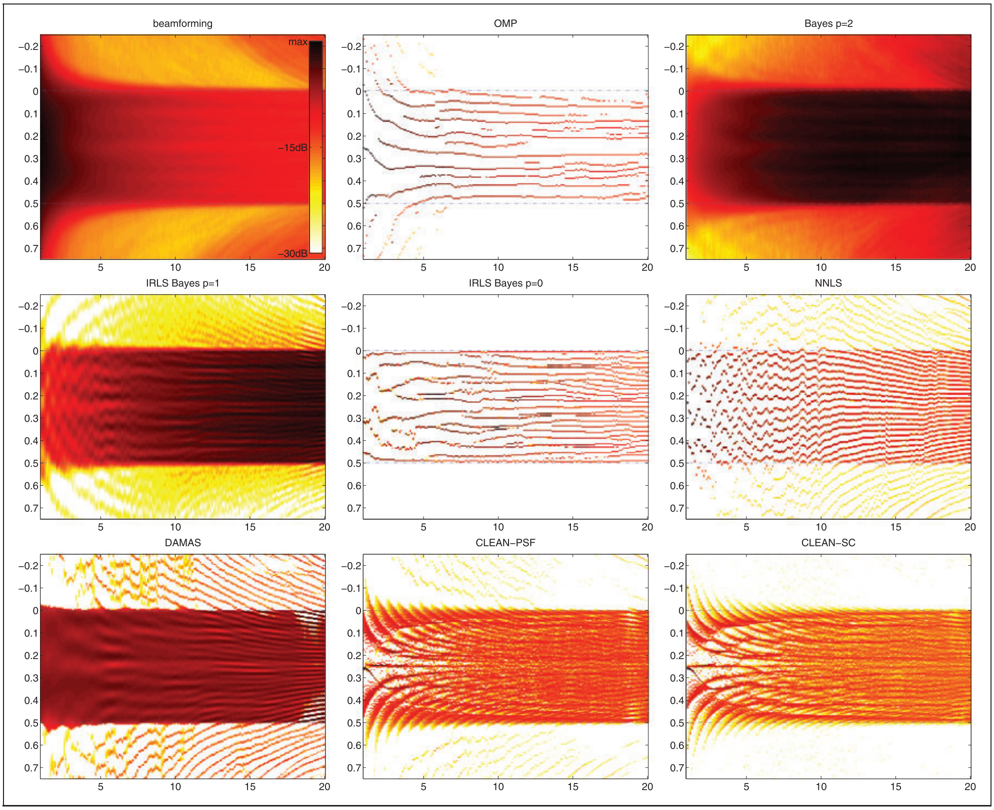

Figure 5. Configuration 3: uncorrelated uniform distribution. Color dynamic 30 dB. Horizontal axis: Frequency in kHz, vertical axis: source position in meters.

frequency range for configuration 4 (correlated distribution). This can be explained by the fact that above 8 kHz, the PSFs of the monopoles of configuration 2 are sufficiently disjoint so that equation (16) is almost valid even for correlated sources (see discussion in 'Deconvolution methods' section). The power estimated using CLEAN-SC is wrong for configurations 2 and 4, because of the correlation between sources. Results of the inverse method with a strong sparsity constraint ($p = 0$) are very similar to deconvolution. Results of OMP for configurations 2 and 4 are very disturbed, highlighting the limitation of heuristic approaches in the case of correlated sources. Results obtained for configuration 2 without or with a soft sparsity constraint ($p = 2$ and 1) are the most reliable, particularly the results of Bayes $p = 1$ which gives a very low error on the whole frequency range.

Application to supersonic jet noise

The various algorithms introduced in this study are now informed with measured pressure signals. The case of an underexpanded supersonic round jet corresponding to an ideally expanded jet Mach number $M_j = 1.35$ is retained to assess these algorithms. The data were simultaneously acquired during a previous study by André et al.,[56] aiming to

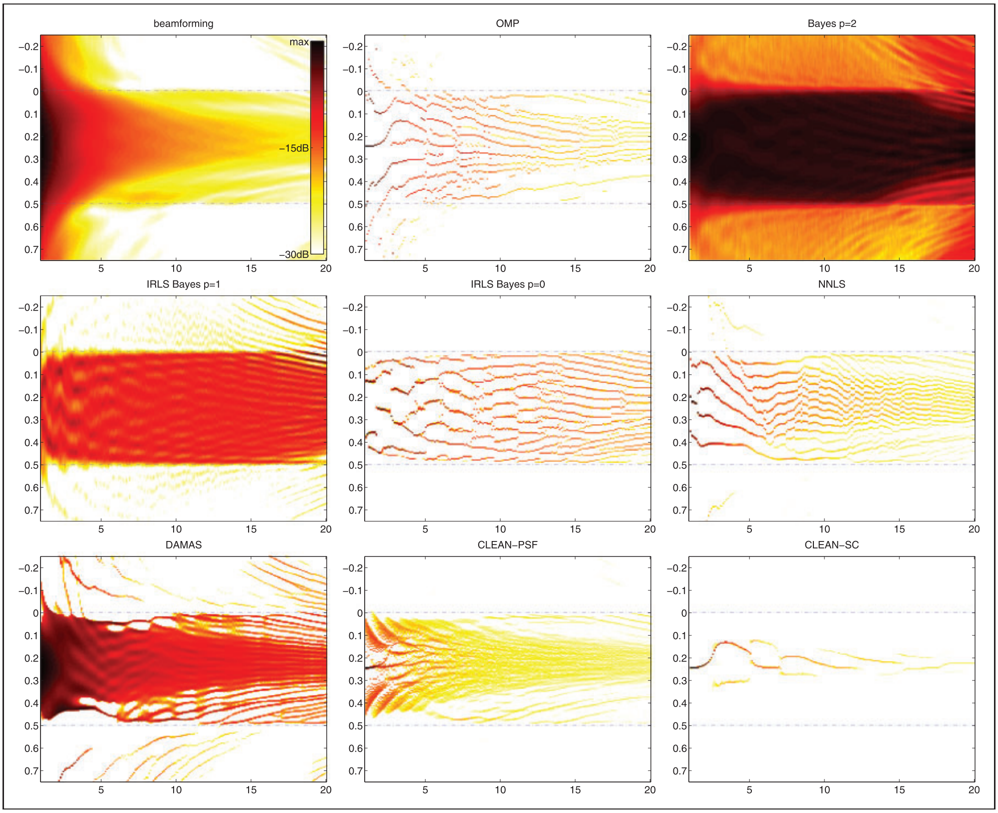

Figure 6. Configuration 4: correlated uniform distribution. Color dynamic 30 dB. Horizontal axis: Frequency in kHz, vertical axis: source position in meters.

characterize the influence of screech on broadband shock-associated noise. The baseline nozzle diameter is $D = 38$ mm, and screech can be removed by using a notched nozzle. A picture of the two nozzles is displayed in Figure 8, the full geometry can be found in André et al.[56]

Experimental setup

The unheated supersonic jet flow originates from a continuously operating compressor mounted upstream of an air drier, and exhausts into the 10 m × 8 m × 8 m anechoic room of the Laboratoire de Mécanique des Fluides et d'Acoustique at Ecole Centrale de Lyon, France. The facility employed in the present study has already been described in André et al.[56,57] Pressure signals are recorded by a one-dimensional array of 32 PCB Piezotronics condenser microphones, mounted in normal incidence without protecting grid. The microphones are irregularly spaced on 70 cm length, as illustrated in Figure 2, in order to optimize the co-array. The linear array is positioned parallel to the jet axis near the nozzle exit, at a radial distance of 0.70 m. All microphone signals are sampled at 51,200 Hz with 30 s duration.

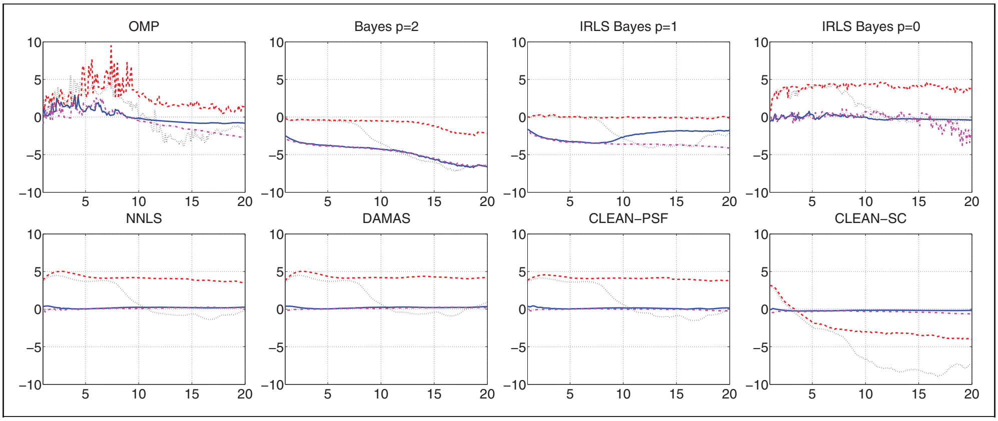

Figure 7. Acoustic power estimation error (estimated/true) in dB. Horizontal axis: Frequency in kHz. Solid blue: uncorrelated monopoles (config. 1). Dotted black: correlated monopoles (config. 2). Dash-dot pink: uncorrelated uniform distribution (config 3). Dashed red: correlated uniform distribution (config. 4).

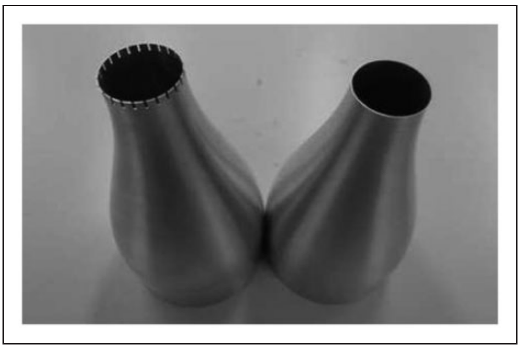

Figure 8. View of the two convergent nozzles: notched nozzle (left) and baseline nozzle (right), taken from André et al.[56]

The efficiency of the notched nozzle as a screech reduction device is illustrated in Figure 9 with the acoustic PSD averaged over all the array microphones. Screech tones can be clearly observed with the baseline nozzle and have been identfied as sinuous mode B.[57] These tones are removed by using the notched nozzle, except for the fundamental frequency $f_s \simeq 3270$ Hz. It must be also pointed out that the two other noise components, that is the mixing noise and the broadband shock-associated noise, are significantly affected by the presence of tones.[56]

Case 1: Baseline nozzle – $M = 1.35$

The algorithms that have been evaluated in 'Numerical illustrations' section by using synthetic data are now applied to the supersonic screeching jet introduced above. The first dataset is obtained with the baseline nozzle. Space-frequency maps are drawn in Figure 10 for all

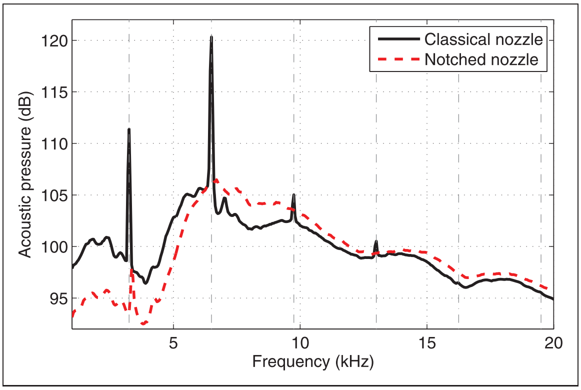

Figure 9. Acoustic PSD (dB/Hz) averaged over the 32 microphones, obtained with the baseline nozzle in solid line, and the notched nozzle in dashed line. The vertical dash-dotted lines indicate screech frequencies.

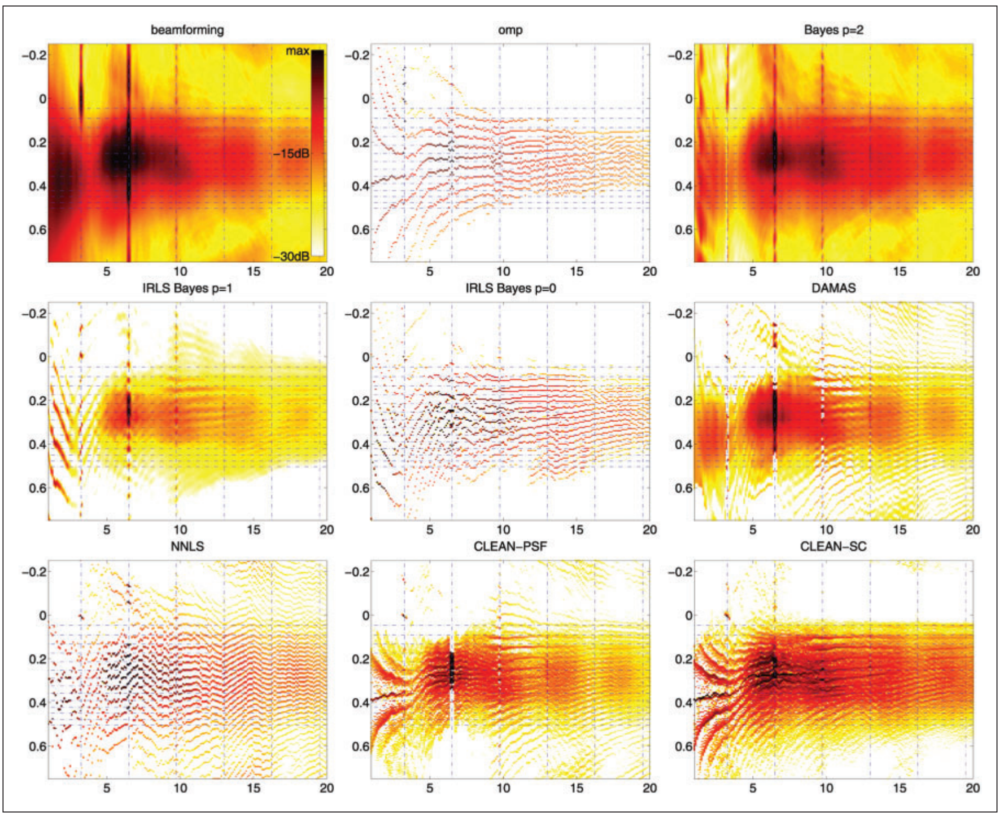

Figure 10. Jet noise result - baseline nozzle – M = 1.35. Horizontal lines: positions of shock cells. Vertical lines: screech frequencies. Color dynamic 30 dB. Horizontal axis: Frequency in kHz, vertical axis: source position in meters.

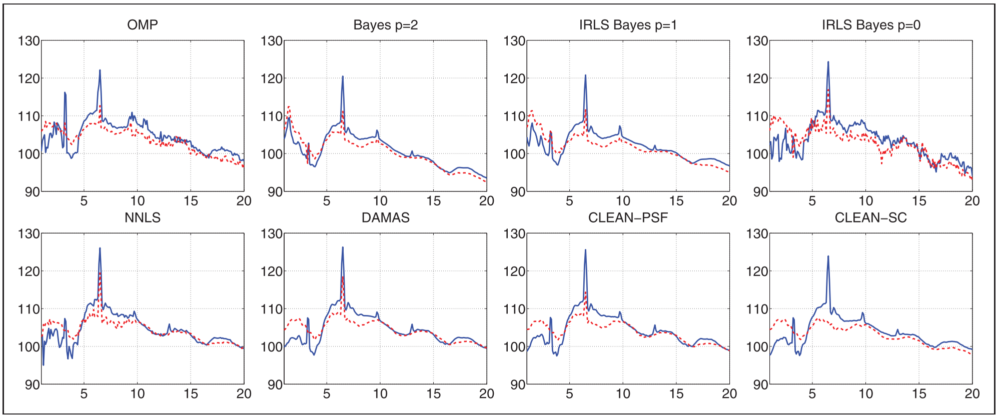

Figure 11. Jet noise result – baseline nozzle – M = 1.35. Acoustic power spectra (dB ref 1e-12 W) of the identified sources integrated for $0 < x < 0.3$ (solid blue), $x > 0.3$ (dashed red). Horizontal axis: Frequency in kHz.

the methods. A first observation, common to all the methods, is that results are very different when looking either on or outside screech harmonics. On harmonics, results are much less distributed, and sometimes exhibit strong sources at positions that are outside the expected source area, for instance around $x = 0$ at the nozzle exit plane for the fundamental frequency at f_s, or between $x = -0.05$ and –0.2 m for the first harmonic at 6500 Hz. This may be due to a specific directivity of the source structure on the second harmonic of screech, with a strong directivity towards the jet axis,[58] generating a potential diffraction contribution by the mock-up. Concerning the broadband noise component, the source energy is well recovered inside the expected source area, between $x = 0$ and $x = 0.5$ m. A maximum is observed in the space-frequency map between around 5 to 12 kHz – $x = 0.15$ to 0.40 cm, for all the methods. A spatial structure is also observed on the broadband shock-associated noise, especially between 8 and 13 kHz, for shock cells #2 to 6. However, the aim of this work is not to analyse deeply the source itself, but only to illustrate the strong diversity of results that are obtained through the different imaging methods. Some methods systematically provide very sparse results (OMP, IRLS $p = 0$, NNLS), and others systematically distributed results (IRLS $p \geq 1$, Capon). Furthermore, DAMAS and CLEAN seem to be able to recover either sparse or distributed sources, which is a very interesting property if the *a priori* of sparsity is not justified for the whole frequency range. In the present case, it may help to separate the broadband shock-associated noise from the contribution linked to the interaction of turbulence with the shock cell structure (that may be rather sparse) from mixing noise (rather distributed).

The integrated acoustic power spectra, estimated as described in 'Acoustic power estimation' section, are displayed in Figure 11. Two integration regions have been defined, $0 < x < 0.3$ (upstream part of the jet) and $x > 0.3$ (downstream part of the jet). Concerning the broadband part of the power spectra, all methods agree that the two regions have equivalent integrated acoustic powers above 10 kHz, and that the upstream and downstream part seem to dominate between 5 and 10 kHz and below 5 kHz, respectively. More discrepancies appear at screech tones: the identified power on the dominant harmonic

(6500 Hz), for instance, varies between about 120 and 126 dB, and its contributions to the two regions of interest are also varying according the different methods.

Case 2: Notched nozzle – $M = 1.35$

The second data-set is obtained with the same underexpanded supersonic jet, but screech tones have been removed thanks to a notched nozzle. The efficiency of such a device has already been quantified in the frequency domain (see Figure 9), and the consequences on the source distribution are assessed by comparing Figures 10 and 12. The same color scale is used to ease these comparisons. The broadband shock-associated noise is slightly shifted towards high frequencies, as already mentioned regarding pressure spectra, but a shift in space in the downstream direction can also be observed. The main lobe between 5 and 12 kHz is now located between $x = 0.2$ and $x = 0.5$ m. The spatial structure related to shock cells is still visible above 9 kHz on almost all maps. However, more cells are visible for this configuration with the notched nozzle, and cells # 4 to 8 seem to be the major sources of jet noise.

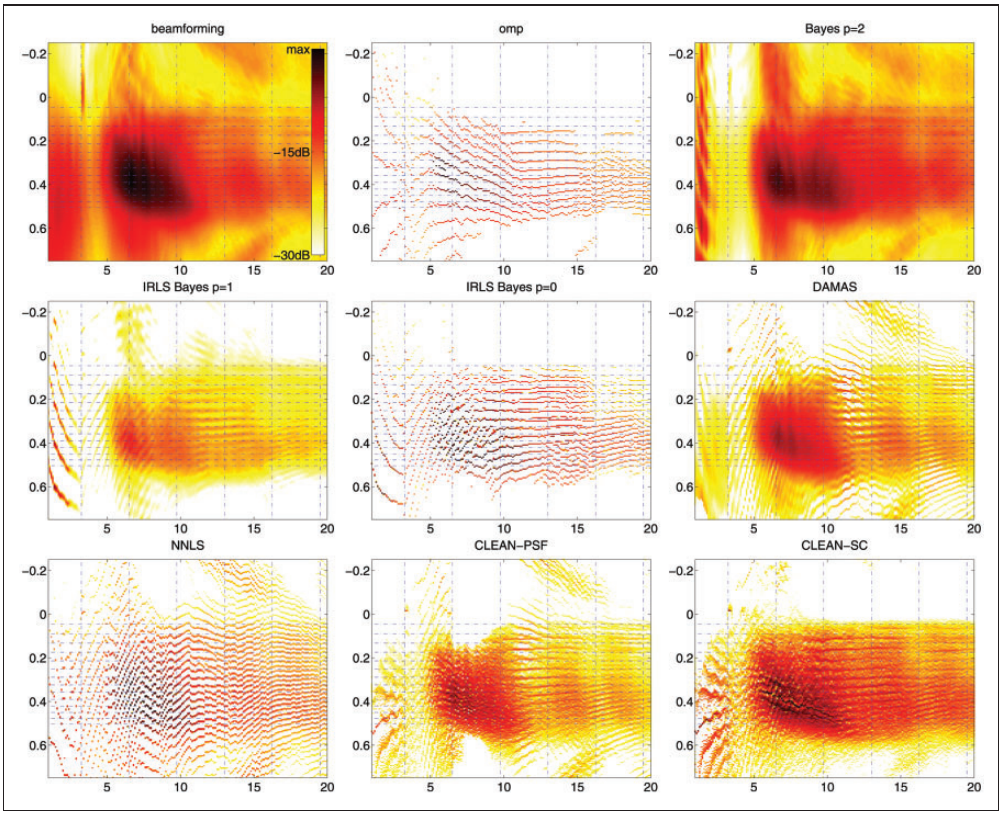

Figure 12. Jet noise result – notched nozzle – M = 1.35. Horizontal lines: positions of shock cells. Vertical lines: screech frequencies. Color dynamic 30 dB. Horizontal axis: Frequency in kHz, vertical axis: source position in meters.

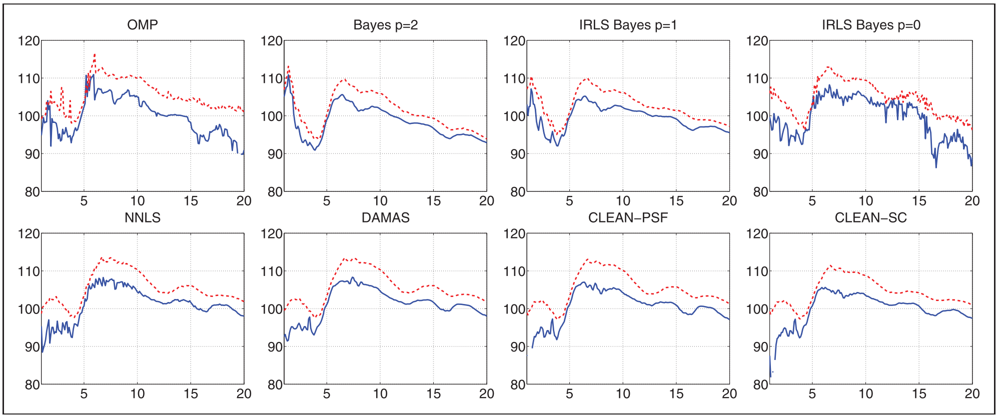

Figure 13. Jet noise result – notched nozzle – $M = 1.35$. Acoustic power spectra (dB ref 1e-12 W) of the identified sources integrated for $0 < x < 0.3$ (solid blue), $x > 0.3$ (dashed red). Horizontal axis: Frequency in kHz.

The acoustic power spectra for the notched nozzle case are drawn in Figure 13. The power is integrated over the same two regions as defined for the baseline nozzle ('Case 1: Baseline nozzle – $M = 1.35$' section). It is clear, comparing Figures 13 and 11, that the center of gravity of the source has been shifted downstream. All methods agree that the acoustic power of the downstream part of the jet is 3 to 6 dB louder than the one of the upstream part. As for the previous case, it seems that the power spectra estimated using inverse methods without or with smooth sparsity (Bayes $p = 2; 1$) are few dBs below the ones estimated by other methods. Inverse methods with strong sparsity constraints (OMP, Bayes $p = 0$) are in good agreement with deconvolution methods up to 16 kHz.

Conclusion

Several acoustic imaging approaches have been presented in this work, with specific effort dedicated to the use of a unified formalism. Some of them have been compared in the frame of a numerical benchmark and of an experimental application, in order to illustrate the diversity of images of an acoustic source that can be obtained through different methods. Results have been also compared quantitatively through integrated acoustic power spectra. It has been shown in the numerical benchmark that the capability of each method to recover a correct power level depends on the application case (incoherent or coherent source distributions). Methods based on the hypothesis of source incoherence (deconvolution methods) do not recover the correct power in case of correlated sources. The capability of inverse methods to recover the correct input acoustic power depends on the amount of sparsity that is enforced. None of the method is able to recover a correct input power for every source configuration. The application to the characterization of a supersonic jet noise is particulary interesting, because the nature of the source distribution depends on the frequency. Sources are expected to be strongly correlated and discrete on screech tones, partially uncorrelated and discrete for broadband shock noise and uncorrelated and distributed for mixing noise. In such a situation, it would be interesting to be able to recover the coherence information as well as the level of sparsity of the real source. Unfortunately, the different methods are based on strong hypothesis concerning these two aspects (correlation and/or sparsity). A pragmatic approach is then to analyse jointly results obtained through different methods in order to avoid errors and bias that could result from the use of a unique approach.

Acknowledgements

This work was performed within the framework of the Labex CeLyA of Université de Lyon, operated by the French National Research Agency (ANR-10-LABX-0060/ANR-11-IDEX-0007).

Declaration of conflicting interests

The author(s) declared no potential conflicts of interest with respect to the research, authorship, and/or publication of this article.

Funding

The author(s) disclosed receipt of the following financial support for the research, authorship, and/or publication of this article: This work was supported by the Labcom P3A (ANR-13-LAB2-0011-01).

References

1. Michel U. History of acoustic beamforming. In: *1st Berlin beamforming conference (BeBeC)*, Berlin, Germany, 21–22 November 2006.
2. Billingsley J and Kinns R. The acoustic telescope. *J Sound Vib* 1976; 48: 485–510.
3. Williams EG, Maynard JD and Skudrzyk E. Sound source reconstructions using a microphone array. *J Acoust Soc Am* 1980; 68: 340–344.
4. Hald J. Basic theory and properties of statistically optimized near-field acoustical holography. *J Acoust Soc Am* 2009; 125: 2105–2120.
5. Wu SF. On reconstruction of acoustic pressure fields using the HELS method. *J Acoust Soc Am* 1998; 104: 1775.
6. Bai MR. Application of BEM (boundary element method)-based acoustic holography to radiation analysis of sound sources with arbitrarily shaped geometries. *J Acoust Soc Am* 1992; 92: 533–549.
7. Flynn OE and Kinns R. Multiplicative signal processing for sound source location on jet engines. *J Sound Vib* 1976; 46: 137–150.
8. Elias G and Malarmey C. Utilisation d'antennes focalisees pour la localisation des sources acoustiques. In: *Proceedings of 11th ICA*. Paris, France, 1927 July 1983.
9. Nelson P and Yoon S. Estimation of acoustic source strength by inverse methods: part I, conditioning of the invese problem. *J Sound Vib* 2000; 233: 639–664.
10. Leclere Q. Acoustic imaging using under-determined inverse approaches: frequency limitations and optimal regularization. *J Sound Vib* 2009; 321: 605–619.
11. Antoni J. A bayesian approach to sound source reconstruction: optimal basis, regularization, and focusing. *J Acoust Soc Am* 2012; 131: 2873–2890.
12. Leclere Q, Le Carrou J-L and Gautier F. Study of a concert harp's radiation using acoustic imaging methods. In: *Proceedings of Acoustics08*. Paris, France, 29 June–4 July 2008.
13. Pereira A and Leclere Q. Improving the equivalent source method for noise source identification in enclosed spaces. In: *Proceedings of ICSV 18*. Rio de Janeiro, Brazil, 10–14 July 2011.
14. Capon J. High-resolution frequency-wavenumber spectrum analysis. *Proc IEEE* 1969; 57: 1408–1418.
15. Stoica P, Wang Z and Li J. Robust capon beamforming. *IEEE Signal Process Lett* 2003; 10: 172–175.
16. Van Trees HL. *Detection, estimation, and modulation theory. Part IV, optimum array processing*. New York: Wiley-Interscience, 2002.

17. Li J, Stoica P and Wang Z. On robust capon beamforming and diagonal loading. *IEEE Transac Signal Process* 2003; 51: 1702–1715.
18. Bienvenu G and Kopp L. Optimality of high resolution array processing using the eigensystem approach. *IEEE Transac Acoust Speech Signal Process* 1983; 31: 1235–1248.
19. Jiang Y and Stoica P. CAPON beamforming in the presence of steering vector errors and coherent signals. In: *Proceedings of the adaptive sensor array processing (ASAP) workshop*, Lexington, MA, USA, 11–13 March 2003.
20. Hadamard J. Sur les problèmes aux dérivées partielles et leur signification physique. *Princeton Univ Bull* 1902; 13: 49–52.
21. Tikhonov A and Arsenine V. *Méthodes de résolution de problèmes mal posés*. Moscou: Mir, 1976.
22. Golub G, Heath M and Wahba G. Generalized cross -validation as a method for choosing a good ridge parameter. *Technometrics* 1979; 21: 215–223.
23. Hansen P. *Rank-deficient and discrete ill-posed problems*. Philadelphia: SIAM, 1998.
24. Pereira A, Antoni J and Leclere Q. Empirical bayesian regularization of the inverse acoustic problem. *Appl Acoust* 2015; 97: 11–29.
25. Pascal J-C and Li J-F. Use of double layer beamforming antenna to identify and locate noise sources in cabins. In: *Proceedings of euronoise*. Tampere, Finland, 30 May – 1 June 2006.
26. Suzuki T. Generalized inverse beam-forming algorithm resolving coherent/incoherent, distributed and multipole sources. In: *14th AIAA/CEAS aeroacoustics conference*, Vancouver, British Columbia, 5–7 May 2008, AIAA paper 2008-2954.
27. Pereira A. *Acoustic imaging in enclosed spaces*. Phd Thesis, INSA de Lyon, France, 2013.
28. Pereira A, Leclere Q, Lamotte L, et al. Noise source identification in a vehicle cabin using an iterative weighted approach to the esm method. In: *Proceedings of ISMA 2012*. Leuven, Belgium, 17–19 September 2012.
29. Bourguignon S, Ninin J, Carfantan H, et al. Exact sparse approximation problems via mixed-integer programming: formulations and computational performance. *IEEE Transac Signal Process* 2016; 64: 1405–1419.
30. Mallat S and Zhang Z. Matching pursuits with time-frequency dictionaries. *IEEE Transac Signal Process* 1993; 41: 3397–3415.
31. Wang Y, Li J, Stoica P, et al. Wideband RELAX and wideband CLEAN for aeroacoustic imaging. *J Acoust Soc Am* 2004; 115: 757–767.
32. Daubechies I, DeVore R, Fornasier M, et al. Iteratively reweighted least squares minimization for sparse recovery. *Commun Pure Appl Math* 2010; 63: 1–38.
33. Chartrand R and Yin W. Iteratively reweighted algorithms for compressive sensing. In: *IEEE international conference on acoustics, speech and signal processing*, Las Vegas, Nevada, 31 March–4 April 2008, pp. 3869–3872.
34. Suzuki T. L1 generalized inverse beam-forming algorithm resolving coherent/incoherent, distributed and multipole sources. *J Sound Vib* 2011; 330: 5835–5851.
35. Zavala P, De Roeck W, Janssens K, et al. Generalized inverse beamforming with optimized regularization strategy. *Mech Syst Signal Process* 2011; 25: 928–939.
36. Le Magueresse T. *Approche unifiee multidimensionelle du probleme d'identification acoustique inverse*. PhD Thesis, INSA de Lyon, France, 2016.
37. Oudompheng B, Pereira A, Picard C, et al. A theoretical and experimental comparison of the iterative equivalent source method and the generalized inverse beamforming. In: *5th Berlin beamforming conference*, Berlin, Germany, 19–20 February 2014.
38. Leclere Q, Pereira A and Antoni J. Une approche bayesienne de la parcimonie pour l'identification de sources acoustiques. In: *Proceedings of CFA*. Poitier, France, 22–25 April 2014.
39. Gill P, Wang A and Molnar A. The in-crowd algorithm for fast basis pursuit denoising. *IEEE Transac Signal Process* 2011; 59: 4595–4605.
40. Tibshirani R. Regression shrinkage and selection via the lasso. *J R Stat Soc Ser B* 1996; 58: 267–288.

41. van den Berg E and Friedlander MP. SPGL1: a solver for large-scale sparse reconstruction, www.cs.ubc.ca/labs/scl/spgl1 (2007, accessed 22 June 2017).
42. Chardon G, Daudet L, Peillot A, et al. Near-field acoustic holography using sparse regularization and compressive sampling principles. *J Acoust Soc Am* 2012; 132: 1521–1534.
43. Blacodon D and Elias G. Level estimation of extended acoustic sources using an array of microphones. In: *9th AIAA/CEAS aeroacoustics conference*, Hilton Head, South Carolina, May 12–14, 2003, AIAA paper 2003-3199.
44. Brooks TF and Humphreys WM Jr. A deconvolution approach for the mapping of acoustic sources (DAMAS) determined from phased microphone arrays. In: *10th AIAA/CEAS aeroacoustics conference*, Manchester, Great Britain, 10–12 May, 2004, AIAA paper 2004-2954.
45. Lawson C and Hanson R. *Solving least squares problems*. Philadelphia: Society for Industrial and Applied Mathematics, 1995.
46. Ehrenfried K and Koop L. Comparison of iterative deconvolution algorithms for the mapping of acoustic sources. *AIAA J* 2007; 45: 1584–1595.
47. Hogbom JA. Aperture synthesis with a non-regular distribution of interferometer baselines. *Astron Astrophys Suppl* 1974; 15: 417–426.
48. Sijtsma P. CLEAN based on spatial source coherence. In: *13th AIAA/CEAS aeroacoustics conference*, Rome, Italy, 21–23 May, 2007, AIAA paper 2007-3436.
49. Padois T and Berry A. Orthogonal matching pursuit applied to the deconvolution approach for the mapping of acoustic sources inverse problem. *J Acoust Soc Am* 2015; 138: 3678–3685.
50. Yardibi T, Li J, Stoica P, et al. Sparsity constrained deconvolution approaches for acoustic source mapping. *J Acoust Soc Am* 2008; 123: 2631–2642.
51. Chu N, Picheral J, Mohammad-djafari A, et al. A robust super-resolution approach with sparsity constraint in acoustic imaging. *Appl Acoust* 2014; 76: 197–208.
52. Bruckstein A, Elad M and Zibulevsky M. On the uniqueness of nonnegative sparse solutions to underdetermined systems of equations. *IEEE Transac Inform Theor* 2008; 54: 4813–4820.
53. Foucart S and Koslicki D. Sparse recovery by means of nonnegative least squares. *IEEE Signal Process Lett* 2014; 21: 498–502.
54. Bendat J and Piersol A. *Engineering applications of correlation and spectral analysis*. New York: Wiley-Interscience, 1980.
55. Leclere Q, Roozen N and Sandier C. On the use of the Hs estimator for the experimental assessment of transmissibility matrices. *Mech Syst Signal Process* 2014; 43: 237–245.
56. André B, Castelain T and Bailly C. Broadband shock-associated noise in screeching and non-screeching underexpanded supersonic jets. *AIAA J* 2013; 51: 665–673.
57. André B, Castelain T and Bailly C. Experimental study of flight effects on screech in underexpanded jets. *Phys Fluids* 2011; 23: 126102.
58. Norum TD. Screech suppression in supersonic jets. *AIAA J* 1983; 21: 235–240.

Appendix

Notation

$\mathbf{A}$ $(n \times n)$ matrix of point spread functions.
$\mathbf{G}$ $(m \times n)$ complex matrix of acoustic transfers.
$\ulcorner \mathbf{L} \lrcorner$ (diagonal $m \times m$) left weighting matrix (real positive).
η regularization parameter.
$\mathbf{p}$ $(m \times 1)$ complex vector of acoustic pressure coefficients.

$\mathbf{P}$	$(m \times m)$ pressure matrix verifying $\mathbf{PP}' = \mathbf{S_p}$.
$\mathbf{q}$	$(n \times 1)$ complex vector of source strength coefficients.
$\bar{\mathbf{q}}^2$	$(n \times 1)$ real positive vector, constituted of diagonal terms of $\mathbf{S_q}$.
$\mathbf{Q}$	$(n \times m)$ source matrix verifying $\mathbf{QQ}' = \mathbf{S_q}$.
$\ulcorner \mathbf{R} \lrcorner$	(diagonal $n \times n$) right weighting matrix (real positive).
$\mathbf{S_p}$	$(m \times m)$ pressure cross spectral matrix.
$\mathbf{S_q}$	$(n \times n)$ source cross spectral matrix.
$\mathbf{S_r}$	$(m \times m)$ residual cross spectral matrix.
w_i	acoustic power associated to the i-*th* source element.
$\mathbf{W}$	$(n \times m)$ complex matrix of source mapping.